Charge Injection Barriers at a Ribonucleic Acid/Inorganic Material Contact Determined by Photoemission Spectroscopy

Niels Dam, Brian V. Doran, J. Chris Braunagel,† and R. Schlaf*

Department of Electrical Engineering, University of South Florida, Tampa, Florida 33620

Received: July 17, 2004; In Final Form: October 16, 2004

Ribonucleic acid (RNA) homopolymer thin films on highly oriented pyrolytic graphite (HOPG) were prepared in ultrahigh vacuum (UHV) directly from aqueous solution by electrospray (ES) injection. The polyadenosine (poly rA) films were prepared in several steps of increasing thickness without breaking the vacuum. Before deposition and between deposition steps, the samples were characterized with photoemission spectroscopy (PES). Both X-ray and ultraviolet photoemission spectroscopy (XPS and UPS) were employed. XPS enabled the detailed measurement of core level peaks, giving insight into the chemical interaction at the interface and the layer morphology. The corresponding UP-spectra sequence allowed us to directly follow the transition from HOPG valence bands to the poly rA highest occupied molecular orbital (HOMO) structure. This enabled the determination of the poly rA ionization energy and work function as well as the charge injection barriers between the Fermi level of the HOPG substrate and the poly rA HOMO. The injection barrier between the lowest unoccupied molecular orbital (LUMO) and the HOPG Fermi level was determined using the HOMO−LUMO gap value determined by optical absorption. The results indicate that significant injection barriers exist between HOPG and the poly rA overlayer, limiting conductivity across this interface.

Introduction

The presented experiments were motivated by the wide spread of results of recent DNA conductivity measurements, ranging from metallic to insulating.[1−5] In these experiments, a variety of contact materials and contacting methods were used. In this context, it appears justified to assume that the nature of the contacts established between electrode and DNA strand probably played a major role in determining the outcomes of these measurements. As is known from small molecular organic and polymeric material interfaces with electrode materials,[6] the nature of the electrode material has a major influence on the magnitude of the charge injection barriers across the interface. In other words, depending on the electrode material, the surface conditions, and the particular nucleotide type in contact, both Ohmic and rectifying contact characteristics might occur at DNA interfaces.

To shed some light on these issues, the experiments presented here focus on the direct determination of the electronic structure of a ribonucleic acid (RNA) contact with an inorganic material using photoemission spectroscopy (PES). The particular system discussed here is the interface between adenosine homopolymer (poly rA) and highly oriented pyrolytic graphite (HOPG). HOPG was selected as the substrate due to its very weak valence band emissions, allowing a detailed measurement of the highest occupied molecular orbital (HOMO) structure of the poly rA polymer. The reason a RNA homopolymer was chosen over a DNA homopolymer lies mostly in the fact that larger quantities can be obtained at reasonable prices, enabling the in-vacuum film deposition using electrospray (ES). Since RNA nucleotides are almost identical in their structure to DNA nucleotides, the presented results also apply to DNA interfaces.

The technique used for the determination of the interface electronic structure was originally developed to characterize charge injection barriers at semiconductor interfaces[7] and has in recent years been expanded to small molecular interfaces.[6,8−13] In the presented experiments, poly rA was deposited in eight steps from aqueous solution on an in-vacuum cleaved HOPG substrate without breaking the vacuum. Since RNA cannot be deposited by in-vacuum evaporation due to the thermal fragility of the molecules, a preparation method based on ES was developed, where the molecules could be introduced into the vacuum chamber directly from their aqueous solution. ES is an established technique used in mass spectroscopy to inject large molecules into spectrometers.[14] To our knowledge, ES has not been used for the in-vacuum deposition of molecular thin films until now. It has, however, been demonstrated that ES can be used at atmospheric pressure to deposit thin films of DNA and other materials, without significant fragmentation.[15−20] Before deposition and after each poly rA deposition step, the sample surface was characterized by X-ray and ultraviolet photoemission spectroscopy (XPS and UPS) to determine the chemical and electronic structure of the prepared thin film. This yielded a sequence of spectra giving step-by-step insight into the formation of the interface. The evaluation of these sequences allowed us to confirm the chemical composition of the overlayer and to determine the charge injection barriers at the poly rA/HOPG interface.

Experimental Section

The experiments were carried out in a commercial multichamber ultrahigh vacuum (UHV) system manufactured by SPECS GmbH (Berlin, Germany) consisting of a fast entry lock, preparation chambers, and an analysis chamber equipped with XPS and UPS. The base pressure of the system was $\sim 2 \times 10^{-10}$ mbar. The homemade ES system was attached to one of the preparation chambers via two differential pumping stages (3.5 mbar and 1.3 mbar pressure during spray operation). Poly rA (Midland Certified Reagent Company, Inc., minimum length

* Corresponding author. E-mail: schlaf@eng.usf.edu.
† Undergraduate research assistant.

10.1021/jp046823i CCC: $30.25
Published on Web 12/16/2004

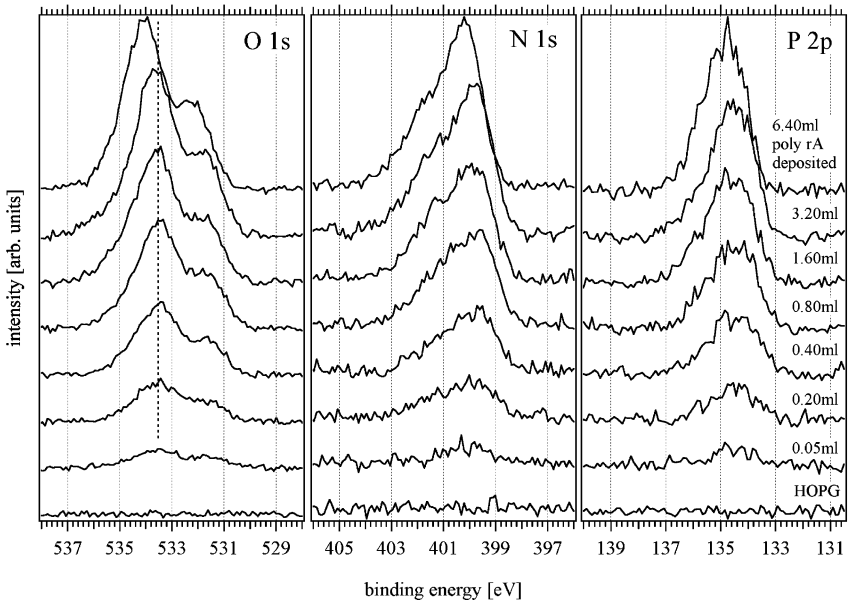

Figure 1. O 1s, N 1s, and P 2p XPS core level spectra measured on the vacuum cleaved HOPG substrate and after each subsequent deposition step. The shift to higher binding energy of the spectra of the final deposition step is a result of charging artifacts.

200 nucleotides, purity better than 95%) was deposited by injecting 1 mg/mL aqueous solution through a 100 μm stainless steal capillary onto the intake orifice (1 mm diameter). The differential pumping stages were separated by 1 mm orifices. The injection rate was 2.0 mL/h. The capillary was held at a bias of −1.5 kV relative to ground. Entry of ambient air into the vacuum system was reduced to insignificant levels by flowing N_2 through the capillary enclosure at slight overpressure relative to atmosphere. Alignment of the injection capillary relative to the intake orifice was achieved using a Faraday cup positionable at the sample position via a retractable feedthrough. Typical currents measured at the sample position were in the range 50−200 pA. During the spray process, the pressure in the deposition chamber rose to $\sim 10^{-5}$ mbar of N_2 pressure, as determined by a residual gas analyzer (RGA). Upon closing the gate valve, separating the ES system from the vacuum chamber, the pressure decreased to $< 5 \times 10^{-8}$ Torr within a few minutes, enabling quick sample transfer to the analysis chamber after each deposition step.

The HOPG substrates (SPI Supplies, grade "SPI-2") were cleaved in situ. This was achieved by attaching a metal foil to the top of the mounted crystal. Using a mechanical manipulator, this foil (including the attached top part of the crystal) was cleaved off in situ, creating a pristine, clean graphite surface. After cleavage and after each of the eight poly rA deposition steps, the sample was characterized by XPS and UPS. The measurements were carried out using a SPECS UVS 10/35 ultraviolet source and a monochromatized SPECS XR 50 X-ray source. The UPS measurements were carried out using the He I ($h\nu = 21.22$ eV) line, while XPS was measured using Al Kα ($h\nu = 1486.6$ eV) excitation. During He I and low intensity XPS work function measurements (see ref 12 for more details on this procedure), a 5 V sample bias was applied to separate sample and analyzer spectral cutoffs and to increase the emission strength of the secondary cutoff. Analysis of the emitted photoelectrons was performed with a SPECS Phoibos 100 hemispherical analyzer. The spectrometer was calibrated to yield the standard Cu $2p^{3/2}$ line at 932.66 eV and the Cu $3p^{3/2}$ line at 75.13 eV.[21]

Atomic force microscopy (AFM) measurements were conducted using a commercial Digital Instruments (Veeco) Dimension 3000 system in tapping mode using Micromasch NSC15 type cantilevers (resonance frequency 325 kHz, force constant 40 N/m). The scan rate was 1 Hz. The AFM data were flattened to remove sample tilt. No further processing was done.

All PES data evaluation was carried out using Igor Pro software (WaveMetrics, Inc.). Where applicable, core level spectra were fitted with Gaussian−Lorentzian profiles using a procedure outlined in ref 22. Work function and HOMO cutoff positions were determined by fitting a line into the spectral onsets and calculating the intersect with the energy axis of the spectra. The given values were corrected for the analyzer broadening (0.2 eV, from Fermi edge width) by adding 0.1 eV to the fitted cutoff values.

Results

Figure 1 shows the O 1s, N 1s, and P 2p XPS lines measured after each poly rA deposition step. The bottom spectra show the spectral regions as measured on the in situ cleaved HOPG substrate for reference. No significant predeposition emissions were detected in the three ranges. The emission lines became immediately visible after the first 0.05 mL deposition step and strongly increased in intensity as the deposition sequence progressed. The emission lines appear to remain at the initial energetic position up to the 3.2 mL deposition step. The spectra of the 6.4 mL step are shifted to higher binding energy by ~0.5 eV, indicating the occurrence of PES induced charging artifacts. The O 1s line shape suggests that at least three independent lines contribute to the signal, with the strongest emission being at 533.7 eV. A line of about half the intensity of the main line is visible at 531.8 eV, and a third line of only weak intensity is located at 535.6 eV. The N 1s line shows a shoulder on the high binding energy side, indicating a second peak at 401.6 eV next to the main peak located at 399.8 eV. The P 2p spectrum appears to be only composed of one fairly broad doublet, with the main $2p^{3/2}$ peak at 134.3 eV and a splitting of 0.96 eV.

Figure 2 shows the C 1s spectral region. The bottom spectrum shows the spectrum representative of the clean HOPG surface. Only one dominant peak together with a weak spread out structure toward high binding energy is visible. The peak at 284.5 is characteristic of HOPG and represents C−C bonds.

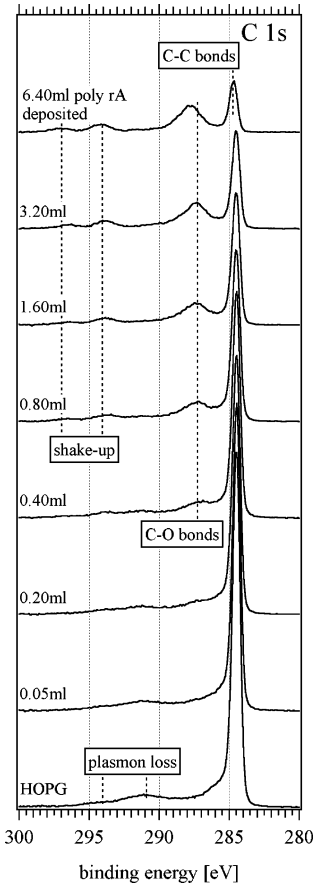

Figure 2. C 1s XPS core level spectra measured on the vacuum cleaved HOPG substrate and after each subsequent deposition step. Besides the C−C bonds related peak at 284.5 eV, poly rA exhibits a secondary peak at ∼287 eV which is related to C−O bonds. Furthermore, two shake-up related peaks arise at 294 and 297 eV as the poly rA overlayer thickness increases.

The weak structure corresponds to plasmon related energy losses incurred by C 1s electrons on their way to the sample surface. The spectra measured after the poly rA deposition steps show a gradual attenuation of the main C 1s peak and a suppression of the plasmon loss feature, while poly rA related emissions emerge. Most notably a wide peak at ∼287.2 eV arises along with two weaker emissions at ∼294 and ∼297 eV, which represent shake-up features (electrons emitted from excited atoms).

Figure 3 shows the UP-spectra sequence corresponding to the XPS data in Figures 1 and 2. The center part of the figure contains the whole spectra as measured. There are three distinct areas in these spectra: (1) HOPG valence bands/poly rA HOMO emissions in the region between the Fermi level (0 eV) and ∼9 eV, (2) emissions from inelastically scattered electrons between 9 eV and the high binding energy cutoff of the spectrum, and (3) the cutoff itself, which allows the determination of the sample work function. The pronounced peak at ∼13.7 eV is related to electrons, which are inelastically scattered into a high density region of the HOPG conduction band, which therefore have a higher probability to leave the sample. The graph on the right side shows the HOMO spectral region with the inelastic background removed to show the HOMO related spectral changes in more detail. It is obvious that the initially weak valence band emissions of the HOPG surface quickly become superimposed by RNA layer related HOMO emissions between 2 and 7 eV. Similar to the XP spectra, a charging related shift becomes apparent as the deposition steps progress. However, in contrast to the shifts observed in the XP spectra of the 6.4 mL deposition step, the shifts begin to occur already after the 0.4 mL deposition step during the UPS measurements. The secondary edge region is shown in more detail on the left side of the figure. Evaluation of the secondary edge shows a marked shift to higher binding energy right after the first deposition step. This is also a result from the occurrence of charging artifacts, which appear most pronounced in the secondary edge feature if lateral layer inhomogeneities are present. This was confirmed by low intensity XPS (LIXPS) secondary edge measurements[12] carried out directly before measuring with UPS, which are shown in Figure 4. These LIXPS measurements were carried out at a very low X-ray intensity, reducing charging effects to insignificant levels, which can be used as a test of

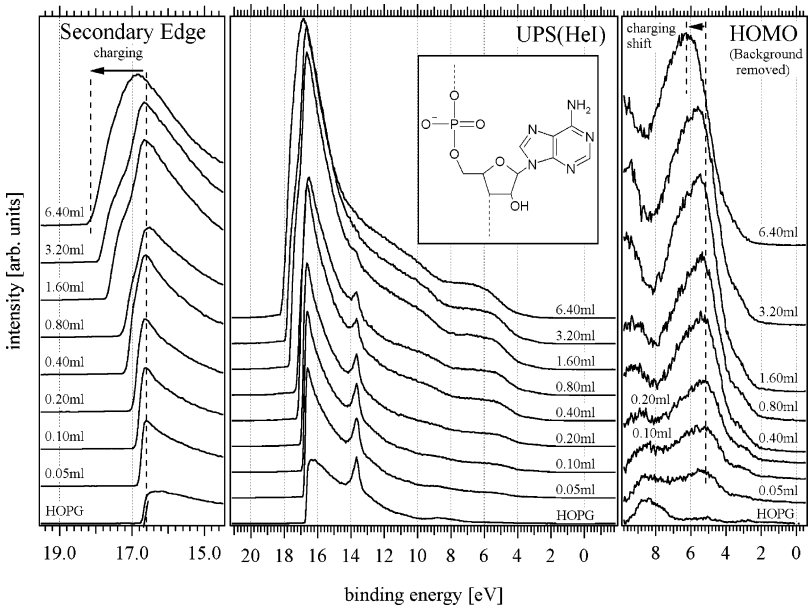

Figure 3. UP spectra corresponding to the XPS spectra series. The graph in the center shows the original spectra. As the poly rA thickness increases, emission features appear between 2 and 11 eV, which are related to the highest occupied molecular orbitals (HOMOs) of poly rA. On the right, the evolution of the main HOMO peak is shown in more detail. On the left, the secondary electron cutoff, which allows one to measure the sample work function, is shown in higher resolution.

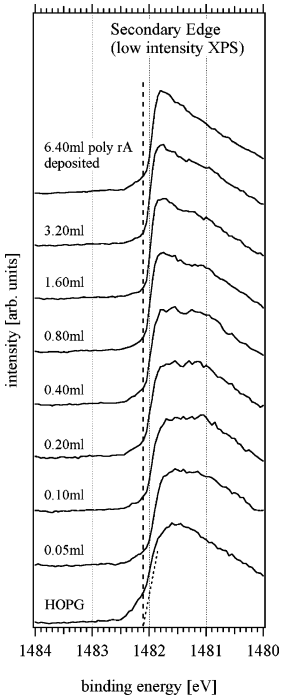

Figure 4. Secondary edge measured with low intensity XPS (LIXPS). In this measurement mode, the X-ray gun is operated at its lowest emission settings, helping to avoid charging artifacts. The absence of any shifts of the secondary edge with increasing layer thickness indicates the absence of charging artifacts during the LIXPS measurements. However, comparison to the shifting UPS secondary cutoff indicates the presence of charging artifacts in the UP spectra.

whether charging artifacts occur in UPS and normal intensity XPS measurements. In contrast to the UPS cutoff, these spectra do not show any shifts, confirming the conclusion that the high intensity ultraviolet light source used in the UPS measurements caused charging artifacts.

Figure 5 shows AFM topographs of $5 \times 5\ \mu m^2$ areas of (left) a freshly cleaved HOPG surface and (right) a 5 mL poly rA thin film on HOPG measured in tapping mode at a scan rate of 1 Hz. The bottom graph shows two representative line scans of each image for comparison (indicated as white lines in the images). The black-to-white height scale of the images is 50 nm. The pristine HOPG surface shows graphene layer steps typical for HOPG. The actual height variations on this sample amount to ~7 nm. The poly rA covered sample shows ringlike features with flat areas in between. The rings are likely a result of droplets impinging on the substrate due to incomplete solvent extraction during the injection process. Statistical analysis of the surface yielded that the ring related features cover ~6% of the surface. The flat areas account for 94%. The ring related features are typically of ~10 nm height relative to the flat areas between, while some areas exceed 20 nm.

Discussion

(A) Stoichiometry. The structure of a poly rA nucleotide unit is shown in the insert of Figure 3. It reveals that each nucleotide unit has 6 O, 5 N, 1 P, and 10 C atoms (H cannot be measured using PES). These ratios should be reflected in the peak intensities of the core level peaks related to each of the atomic species. The particular chemical environment of each individual atom finds its expression in shifted peak positions. Since it appears that during the XPS measurements significant charging effects only occurred after the last deposition step (no significant peak shifts after earlier steps), the spectra of the 3.4 mL deposition step were used for a detailed spectral analysis

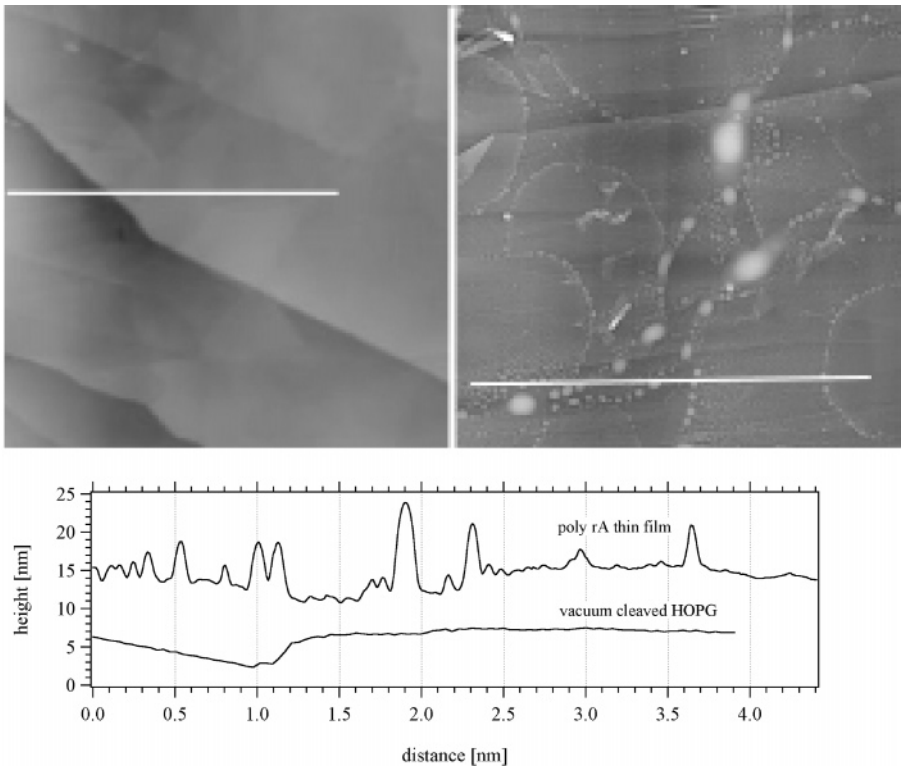

Figure 5. Tapping mode atomic force microscopy (TMAFM) topographs of (left) a pristine HOPG surface and (right) a poly rA thin film (from 5 mL deposition) on HOPG. The shown scan areas are $5 \times 5\ \mu m^2$. The HOPG sample shows the typical graphene layer related steps, while the ringlike features on the poly rA film are likely a result of the occasional deposition of only partially evaporated droplets on the sample surface. The bottom graph shows two representative line scans from each of the images (indicated in images as white lines) for direct comparison of feature heights.

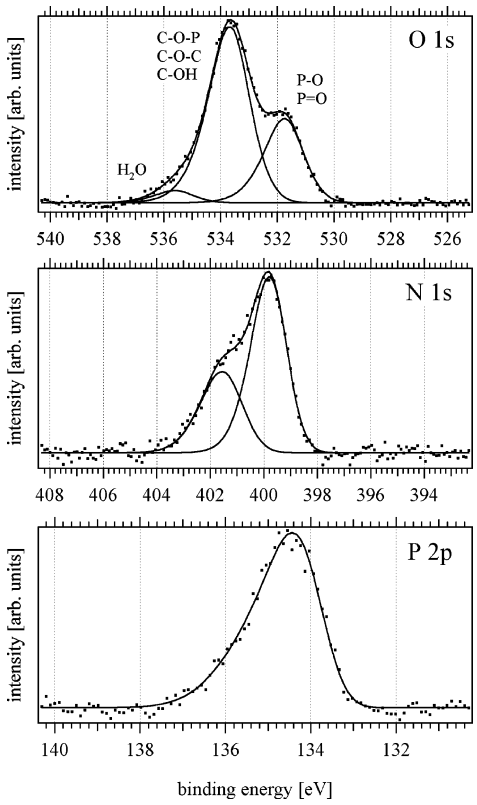

Figure 6. O 1s, N 1s, and P 2p spectra measured after the 3.2 mL deposition step with fitted Gaussian−Lorentzian peak shapes.

by peak fitting, since they offer the best signal-to-noise ratio. Figure 6 shows the O 1s, N 1s, and P 2p peaks of the 3.4 mL step magnified with fitted peak shapes.

The O 1s spectrum shows two main peak features with a weak shoulder occurring on the high binding energy side of the spectrum. The symmetrical Gaussian−Lorentzian line shapes that were fitted have a full width at half-maximum (fwhm) of 1.7 eV and are located at 531.8, 533.7, and 535.6 eV. Of the 6 O atoms in adenosine, two are bonded to the central P atom of the phosphate unit in the backbone, while the other four are either bonded to two C atoms or bonded to the P atom and one C atom. The intensity ratio between the main O 1s peak at 533.7 eV and the secondary peak at 531.8 eV was determined to be 2.08:1, suggesting that the weaker peak originates from the O atoms in the phosphate unit, while the main peak is related to the O atoms bonded to C and P atoms. This assignment is supported by published results[23] on various polymers where the O 1s binding energy for C−O−P structures was measured at 533.37 eV, and for C−O−C structures at energies ranging from 532.94 to 533.59 eV. O atoms in phosphates, on the other hand, are known to yield O 1s peak positions in the range 530.5−532.5 eV,[24] confirming the assignment of the secondary peak. The weak shoulder that was fitted with a small peak at 535.6 eV might be related to adsorbed water, which exhibits peak positions around 535 eV.[24] This is a likely explanation, since water was used as the solvent during the experiments, and it can be assumed that a small amount of water makes it through the ES system during deposition. An analysis of the peak intensity yields a ratio of 1:14 relative to the main peak. Taking into account that the main peak relates to four atoms per nucleotide unit, one can estimate that approximately one water molecule was adsorbed per 3.5 nucleotide units. This analysis is, however, not supported by an analysis of the peak intensities where a slight O deficiency was found (see below).

The center graph of Figure 6 shows the fit performed on the N 1s emission. A good fit was obtained with two symmetrical Gaussian−Lorentzians at 399.8 and 401.6 eV with a 2.17:1 intensity ratio and fwhm values of 1.65 eV (main peak) and 1.91 eV (secondary peak). The resulting area ratio (by multiplying intensities with fwhm values) is 1.9:1 between the main and secondary peaks. It turned out that the analysis of the N 1s emissions is not as straightforward as that of the O 1s emission, since it is difficult to assign the emission lines unanimously. Of the five N atoms in the adenine base, three are in very similar chemical environments, bonded to two C atoms each. The fourth N atom is also bonded to two C atoms on the base but is also bonded to the ribose unit on the backbone. The fifth N atom is located in the amino group attached to the adenine unit. From XPS results on thiolated thymidine homopolymers self-assembled on a gold surface,[25] it appears that the N atoms on the rings and the one bonded to the ribose unit all yield N 1s emissions at ∼401 eV, which would allow us to assign the secondary peak to the N atoms on the adenine rings. From measurements on polymers featuring $-NH_2$ ligands,[26] it is known that the N 1s emission associated with these units occurs at ∼400 eV, which would match the position of the main peak measured in here. Unfortunately, the intensity ratios between the measured peaks do not match this assignment, which should yield a 4 times stronger secondary peak than the main peak. At this point, we do not have a good explanation of this phenomenon, which needs more investigation.

The bottom graph of Figure 6 shows the fit to the P 2p line, which could be successfully matched by a single 2:1 intensity ratio doublet, as would be expected for a p-orbital related line. The locations of the P $2p^{3/2}$ and $2p^{1/2}$ peaks were found to be at 134.3 and 135.2 eV. The fwhm of the peaks is 1.4 eV. The assignment of a single doublet is reasonable, since there is only one P atom per nucleotide.

The C 1s emissions are shown in Figure 2. Due to the superimposed emissions from the graphite substrate, which is composed of 100% carbon, only the emissions of carbon not related to C−C bonds can be evaluated. From ref 27, it is known that the ribose and phosphate units both yield emission lines at around 285 and 287 eV. These lines are also present in the spectra presented here. In addition, we note emissions at 294 and 297 eV, which are related to shake-up features originating from electrons emitted from excited atoms.

An analysis of the integrated peak areas of the O 1s, N 1s, P 2p, and C 1s lines was carried out using the following relation to adjust the measured areas (A) for ionization cross section (CS), analyzer transmission function (TF), and mean free path (MFP) of the emitted electrons to obtain absolute intensities ($I_{absolute}$):

$$I_{absolute} = \frac{A}{CS \cdot TF \cdot MFP} \tag{1}$$

As CS values, the values calculated by Scofield were used.[28] The TF was approximated by

$$TF = \frac{1}{\sqrt{E_{kin}}} \tag{2}$$

where E_{kin} is the kinetic energy of the emitted electrons. E_{kin} dependent MFP values were interpolated from the values tabulated by Tilinin et al.[29]

Table 1 gives the values used and the calculated absolute intensities normalized such that P 2p has an intensity of $I_{absolute}(P\ 2p) = 1$. The absolute intensity ratios between P 2p

TABLE 1: Values Used to Calculate Absolute Peak Intensities for Stoichiometry Evaluation[a]

	peak area (A)	cross section (CS)	mean free path (MFP), Å	kinetic energy (E_{kin}), eV	transmission factor (TF)	normalized absolute intensity ($I_{absolute}$)
N 1s	1970	1.8	28	1086	0.030	4.2
O 1s	4328	2.93	26	956	0.032	5.7
P 2p	333	1.18	34	1351	0.027	1
C 1s	4245	1.0	31	1202	0.029	15

[a] The absolute intensities are given normalized relative to the P 2p peak area.

and O 1s (5.7:1) and N 1s (4.2:1) are somewhat too low but still consistent with the composition of poly rA taking the typical accuracy of PES stoichiometry determinations (~10−20%, if no standards are used) into account. In contradiction to the peak shape evaluation above, the O 1s ratio does not support the conclusion that water was present in the deposited layers. However, in light of the stoichiometry accuracy of PES, it appears justified to assume that the peak shape analysis bears a larger weight and that a small amount of water has been present in the films. The stoichiometry results are also confirmed by the peak area values published by May et al. obtained on adenosine DNA oligomers.[27] Their results also show somewhat lower O 1s and N 1s values relative to P 2p (5.3:1 and 4.0:1) than what would be justified stoichiometrically (6:1 and 5:1). Their ratio for C 1s/P 2p is 13.5:1, which is too high compared to the 10:1 stoichimetric ratio. It was concluded that the additional C 1s emissions were related to the ambient contamination present on their samples due to the ex situ preparation process. In contrast, the results presented here yield a C 1s/P 2p ratio of 15:1, which, while also being too high, is rather a result of the superposition of the C 1s emissions of the HOPG substrate instead of contamination.

(B) Interface Morphology. The standard method for the evaluation of thin film thickness based on PES measurements is to use an exclusively substrate related core level peak and analyze its intensity attenuation depending on the overlayer thickness. Unfortunately, this is not possible in the presented experiment due to the spectral overlap of substrate and poly rA overlayer C 1s emissions. The only purely substrate related emission feature is the 13.7 eV peak in the UP spectra. Figure 7 shows this peak magnified with its background removed (the method used was to fit a second-order polynomial into the surrounding background signal). It is obvious that the peak becomes strongly attenuated as the deposition sequence is completed. The last two spectra are similar in intensity, indicating that the layer has reached a thickness where the substrate emissions are completely attenuated. They also suggest that poly rA also has some weak emissions in this range due to its aromatic rings (similar observations were made in other experiments where chloroindium phthalocyanine (ClInPc) thin films were deposited on HOPG[30]).

Using an exponential decay function for the attenuation of substrate related emissions through the deposited overlayer,

$$I = I_0 \exp\left(-\frac{d}{\mathrm{MFP}}\right) \tag{3}$$

where I is the intensity of the emission line after deposition, I_0 its intensity measured on the uncovered substrate, d the thickness of the overlayer, and MFP the mean free path of the emitted electrons. Solving the equation for d, one obtains

$$d = -\mathrm{MFP} \ln\left(\frac{I}{I_0}\right) \tag{4}$$

Figure 8 plots the thickness values (d) calculated with eq 4 using a mean free path of 28 Å for electrons of ~7.5 eV kinetic energy[31] (a measured binding energy of 13.7 in an He I UP spectrum corresponds to 7.5 eV kinetic energy) versus the injected volume of poly rA solution. The ratio I/I_0 was obtained from the peak areas. The graph shows an initially almost linear increase of the layer thickness with deposited volume, indicating flat layer-by-layer growth. At 3.2 mL, the curve goes into a plateau, which is caused by the weak poly rA related emissions. With regard to the thickness evaluation attempted here, these two data points need to be discarded. The slope of the line fitted into the linear part of the curve yields a deposition rate of 21 Å/mL during the ES deposition process. This suggests that the final layer thickness after the deposition of 6.4 mL was 134 Å. The AFM data shown in Figure 5 essentially confirms the layered growth mode. While ring-shaped areas of ~10−20 nm height were observed, most of the surface appears covered by a flat layer. The ring features only cover 6% of the total surface area. This means they only contribute to 6% of the measured signal; that is, they have no significant influence on the peak areas and positions. The only feature where these areas of increased height play a significant role is the secondary edge, which is shifted by charging artifacts occurring on these areas (see below). The reason for the occurrence of the ringlike features is probably the result of an occasional deposition of

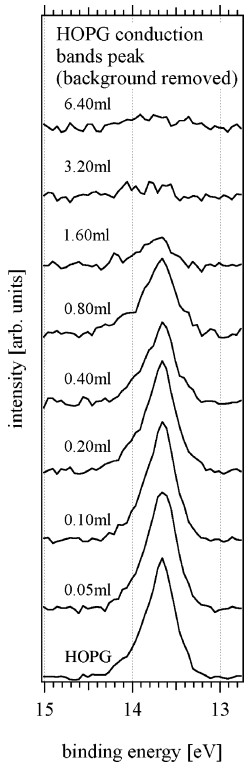

Figure 7. UPS peak at 13.7 eV with the background removed for peak area determination. This peak is related to the conduction band density of states in the HOPG substrate. It represents the only purely HOPG related emission feature, which can be used for the layer thickness determination to calibrate the deposited amount of poly rA per injected solution volume.

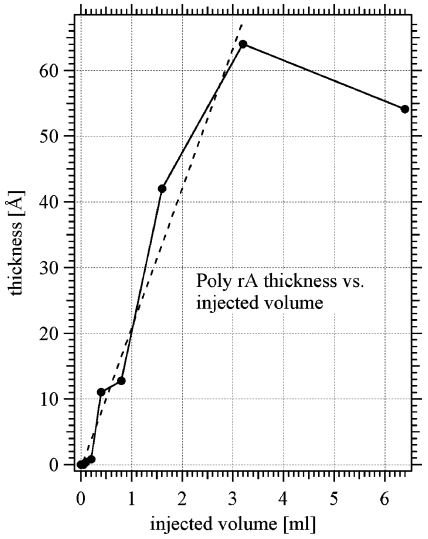

Figure 8. Poly rA layer thickness determined from the 13.7 eV UPS emission line. During the first deposition steps, an almost linear thickness increase occurred which was fitted with a line, yielding a deposition rate of 21 Å/mL.

droplets, which did not completely dissipate in the differential pumping stages during the injection process.

(C) Electronic Structure. The electronic structure of the poly rA interface can be determined from the spectra sequence of the HOMO emission region of the UP spectra. However, in the case of potentially poorly conductive materials such as RNA, the possibility of the occurrence of charging artifacts needs to be taken into account. A comparison of the shifts of the secondary edge cutoff of the UP spectra shown in Figure 3 with the constant position of the low intensity XPS cutoffs shown in Figure 4 suggests that already immediately after the first deposition step charging occurs to a certain degree. The amount of charging in the UP cutoff ranges from 0.1 eV after the first deposition step to 0.25 eV after the 0.2 mL step to finally 1.4 eV after the 6.4 mL step. On the other hand, the HOMO peak maximum remains at the same position up to the 0.4 mL step and then only slowly begins to drift to higher binding energy, ending at a total shift of ~1.0 eV. The discrepancy between cutoff and HOMO shifts can be explained by assuming that areas exhibiting different magnitudes of charging artifacts are present on the surface. Such an assumption appears justified due to the presence of the ringlike features, which cover a small amount of the surface but are likely to exhibit stronger charging artifacts than the flat regions due to their larger height. While primary emission features such as the HOMO peak are a true superposition of all areas on the surface, that is, represent an average of the various emission regions, the secondary cutoff feature emphasizes the areas yielding the slowest electrons, that is, the most highly charged areas. In other words, a small amount of areas showing stronger charging effects will strongly influence the cutoff position, while their influence on the HOMO position may still be relatively small. Furthermore, as long as the area contributing to strong charging effects is small, peak features will only become distorted on the high binding energy side, while their onset on the low binding energy side remains unchanged and only changes its slope but not its position. These considerations allow us to use the 0.2 mL spectrum for the evaluation of the HOMO position, since the contributions from charged regions appear not to be significant enough at this coverage level to cause significant shifts of the onset of the peak.

Figure 9 shows the detailed evaluation of the 0.2 mL HOMO spectrum. The top part shows the original data with the fitted

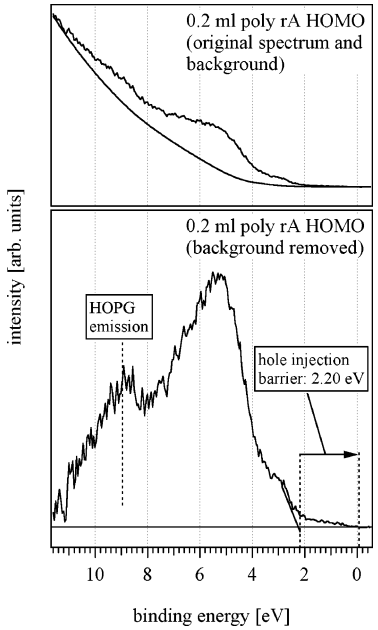

Figure 9. Evaluation procedure of the highest occupied molecular orbital (HOMO) cutoff for the determination of the charge injection barriers at the interface. (top) UP spectrum of the 0.2 mL deposition step shown together with its inelastic background. (bottom) UP spectrum after background removal. The line fitted to the low binding energy cutoff of the HOMO peak is shown schematically. An energy difference of 2.20 eV was determined between the HOMO cutoff and the substrate Fermi level at 0 eV.

background signal. The background was obtained by fitting the integral of the original spectrum to the background areas surrounding the HOMO emission features.[12] The bottom graph shows the spectrum after background removal. Three main emission features are visible. The secondary peak at high binding energy is superimposed emission from the HOPG substrate. The main peak and the shoulder on the low binding energy side are poly rA related emissions. The weak tail toward the Fermi edge at 0 eV is also HOPG related and represents valence band states below the Fermi edge. The cutoff of the HOMO emissions was determined by fitting a straight line into the onset and determining its intersect with the binding energy axis. This evaluation yielded a value of 2.10 eV, which, after correction for the analyzer broadening of 0.1 eV, allowed us to conclude that the hole injection barrier (Φ_h) between HOPG and poly rA amounts to 2.20 eV.

The evaluation of the low intensity XPS cutoffs shown in Figure 4 indicates that no significant interface dipole arose between poly rA and HOPG. This is apparent from the absence of any shifts of the cutoff, indicating that no significant local charge transfer at the interface occurred as the poly rA layer formed. Such a conclusion is supported by the inert nature of HOPG resulting only in the formation of van der Waals bonds at the interface to organic materials, rather than the formation of chemical bonds. Similar results were obtained in earlier experiments, where other organic materials were deposited on HOPG, and no significant interface dipoles were found.[30,32]

Using a value of $E_g = 4.8$ eV for the HOMO−lowest unoccupied molecular orbital (LUMO) gap determined by UV absorption,[33] the electron injection barrier (Φ_e) between the HOPG Fermi level and the poly rA LUMO can be estimated by subtracting the hole injection barrier (Φ_h). Using this estimation, a value of $\Phi_e = 2.6$ eV was calculated. This value should be considered a lower threshold for the electron injection barrier, since optical absorption generally measures the elec-

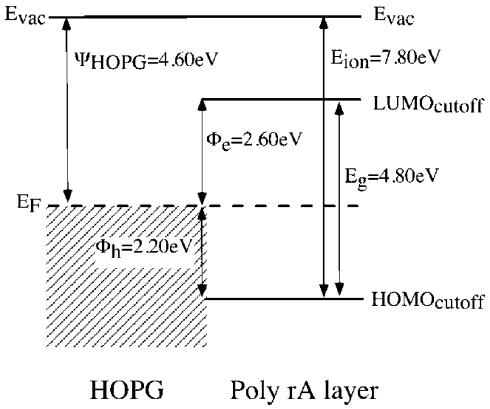

Figure 10. Summary of the electronic structure of the poly rA/HOPG interface as determined from the UP-spectra series. The work function (Ψ) of the HOPG substrate was determined to be 4.60 eV. No dipole potential is present at the interface, resulting in an unchanged work function in the poly rA layer. The hole injection barrier between the HOPG Fermi level and the poly rA HOMO (Φ_h) was determined to be 2.20 eV, while the corresponding electron injection barrier (Φ_e) amounts to 2.60 eV if the HOMO−LOMO gap, $E_g = 4.80$ eV, is taken into account. Adding the hole injection barrier and the work function, an ionization energy of $E_{ion} = 7.80$ eV was determined for the poly rA thin film.

tronic gap minus the exciton binding energy, which can be considerable (several tenths of electronvolts) in organic materials.[34] Unfortunately, to our knowledge, no exciton binding energies have been determined for RNA to date. The work function of the HOPG substrate was determined to be 4.60 eV by subtracting the binding energy of the secondary cutoff of the initial UP spectrum of the clean HOPG surface from the excitation energy of the He I line, 21.21 eV, and correcting it for the analyzer broadening by adding 0.1 eV.

The results of the electronic structure evaluation are shown summarized in Figure 10. The vacuum level is a straight line across the interface due to the absence of significant interface dipoles. This suggests that this interface obeys the Schottky−Mott rule;[35,36] that is, the injection barriers correspond to the difference between the metal (HOPG) work function and the semiconductor (RNA) ionization energy or electron affinity. The poly rA polymers align in a way that the Fermi level of the HOPG substrate is close to the center of the HOMO−LUMO gap. By adding the hole injection barrier (Φ_h) to the HOPG work function, an ionization energy (E_{ion}) of 7.80 eV was determined for the poly rA layer.

The large charge injection barriers suggest that the interface has probably poor charge transfer characteristics in both directions. This is supported by the early onset of charging artifacts in the PES measurements, which indicate that the transport across the interface is the main inhibition for the charge transport, rather than transport through the deposited layer itself. Considering these results, it may be speculated that conductivity measurements carried out on oligonucleotides contacted by various kinds of metal electrodes may also be influenced by contacts of non-Ohmic character. However, further PES measurements on metal/nucleotide interfaces will be necessary to draw final conclusions.

With regard to measurement errors, it should be noted that often an error margin of $\sim \pm 0.1$ eV is assigned to absolute energy value photoemission measurements. These errors are mainly a result of slight differences in the calibration of the particular instrumentation used. This absolute error margin is not crucial for the determination of charge injection barriers, since in this case only differences between absolute values are used. However, the evaluation of the spectral cutoffs (secondary edge and HOMO cutoff) used for the determination of the charge injection barriers also depends on the way the lines are fitted into the cutoff features, which may be a source of error. We estimate that in the case of the HOMO and secondary cutoffs the assumption of an error margin of ± 0.1 eV is probably justified, while the Fermi edge position can be determined with much better accuracy (± 0.03 eV). On particular equipment, XPS core level peak positions can be determined very accurately due to the well-defined peak shapes in combination with very precise peak fitting procedures. We estimate that the error margins in relative peak positions are $\sim \pm 0.05$ eV, which gives an absolute error margin of $\sim \pm 0.11$ eV.

Conclusion

A thin film of polyadenosine (poly rA) homopolymer was deposited in eight steps on a highly oriented pyrolytic graphite (HOPG) substrate without breaking the vacuum. This was achieved by employing electrospray (ES) deposition, which allowed the introduction of poly rA into the vacuum chamber directly from solution. Photoemission spectroscopy (PES) measurements before and between poly rA deposition steps gave a detailed account of the formation of the interface between the two materials. Stoichiometry, interface morphology, and interface electronic structure were determined from the measurements. The stoichiometric results confirm results previously measured by other groups on DNA thin films using X-ray photoemission spectroscopy (XPS). The presented ultraviolet photoemission spectroscopy (UPS) measurements revealed the highest occupied molecular orbital (HOMO) structure of poly rA, and the orbital lineup at the interface to HOPG. The results indicate the formation of a dipole-free interface with significant charge injection barriers.

Acknowledgment. Financial support by the National Science Foundation (grant DMR 0205577), the Petroleum Research Fund (grant 38584-AC7), and the Semiconductor Research Corporation (grant 2000-RJ-868G) is gratefully acknowledged. J.C.B. acknowledges partial funding through an Engineering Undergraduate Research Fellowship provided by the USF College of Engineering Research Experience for Undergraduates program. We are grateful to M. M. Beerbom and B. Lägel for technical support and helpful discussions.

References and Notes

(1) Fink, H. W.; Schonenberger, C. *Nature* **1999**, *398* (6726), 407−410.
(2) Porath, D.; Bezryadin, A.; de Vries, S.; Dekker, C. *Nature* **2000**, *403* (6770), 635−638.
(3) Cuniberti, G.; Craco, L.; Porath, D.; Dekker, C. *Phys. Rev. B* **2002**, *65* (24).
(4) Storm, A. J.; van Noort, J.; de Vries, S.; Dekker, C. *Appl. Phys. Lett.* **2001**, *79* (23), 3881−3883.
(5) Cai, L. T.; Tabata, H.; Kawai, T. *Appl. Phys. Lett.* **2000**, *77* (19), 3105−3106.
(6) Ishii, H.; Sugiyama, K.; Ito, E.; Seki, K. *Adv. Mater.* **1999**, *11* (8), 605−625.
(7) Waldrop, J. R.; Grant, R. W. *Phys. Rev. Lett.* **1979**, *43* (22), 1686−1689.
(8) Hill, I. G.; Rajagopal, A.; Kahn, A.; Hu, Y. *Appl. Phys. Lett.* **1998**, *73* (5), 662−664.
(9) Schlaf, R.; Parkinson, B. A.; Lee, P. A.; Nebesny, K. W.; Armstrong, N. R. *J. Phys. Chem.* **1999**, *103*, 2984−2992.
(10) Hill, I. G.; Mäkinen, A. J.; Kafafi, Z. H. *J. Appl. Phys.* **2000**, *88* (2), 889−895.
(11) Schlaf, R.; Merritt, C. D.; Picciolo, L. A.; Kafafi, Z. H. *J. Appl. Phys.* **2001**, *90* (4), 1903−1910.
(12) Schlaf, R.; Merritt, C. D.; Crisafulli, L. A.; Kafafi, Z. H. *J. Appl. Phys.* **1999**, *86* (10), 5678−5686.

(13) Schlaf, R.; Schroeder, P. G.; Nelson, M. W.; Parkinson, B. A.; Lee, P. A.; Nebesny, K. W.; Armstrong, N. R. *J. Appl. Phys.* **1999**, *86* (3), 1499−1509.

(14) Cole, R. B. *Electrospray Ionization Mass Spectrometry: Fundamentals, Instrumentation, and Applications*; John Wiley & Sons: New York, 1997.

(15) Vanderei, W.; Oldenhof, W.; Zehner, W. *Nucl. Instrum. Methods* **1973**, *112* (1−2), 343−351.

(16) Lowentha, Gc.; Wyllie, H. A. *Nucl. Instrum. Methods* **1973**, *112* (1−2), 353−357.

(17) Lauer, K. F.; Verdingh, V. *Nucl. Instrum. Methods* **1963**, *21* (1), 161−166.

(18) Morozov, V. N.; Morozova, T. Y. *Anal. Chem.* **1999**, *71* (15), 3110−3117.

(19) Festag, R.; Alexandratos, S. D.; Joy, D. C.; Wunderlich, B.; Annis, B.; Cook, K. D. *J. Am. Soc. Mass Spectrom.* **1998**, *9* (4), 299−304.

(20) Festag, R.; Alexandratos, S. D.; Cook, K. D.; Joy, D. C.; Annis, B.; Wunderlich, B. *Macromolecules* **1997**, *30* (20), 6238−6242.

(21) Seah, M. P. *Surf. Interface Anal.* **1989**, *14*, 488.

(22) Kojima, I.; Kurahashi, M. *J. Electron. Spectrosc. Relat. Phenom.* **1987**, *42*, 177.

(23) Briggs, D.; Beamson, G. *Anal. Chem.* **1993**, *65* (11), 1517−1523.

(24) Moulder, J. F.; Stickle, W. F.; Sobol, P. E.; Bomben, K. D. *Handbook of X-ray Photoelectron Spectroscopy*; Physical Electronics, Inc.: Eden Prairie, MN, 1995.

(25) Petrovykh, D. Y.; Kimura-Suda, H.; Whitman, L. J.; Tarlov, M. J. *J. Am. Chem. Soc.* **2003**, *125* (17), 5219−5226.

(26) Jones, T. S.; Ashton, M. R.; Richardson, N. V.; Mack, R. G.; Unertl, W. N. *J. Vac. Sci. Technol., A* **1990**, *8* (3), 2370−2375.

(27) May, C. J.; Canavan, H. E.; Castner, D. G. *Anal. Chem.* **2004**, *76* (4), 1114−1122.

(28) Scofield, J. H. *J. Electron. Spectrosc. Relat. Phenom.* **1976**, *8*, 129.

(29) Tilinin, I. S.; Jablonski, A.; Werner, W. S. M. *Prog. Surf. Sci.* **1996**, *52* (4), 193−335.

(30) Schlaf, R.; Parkinson, B. A.; Lee, P. A.; Nebesny, K. W.; Armstrong, N. R. *Surf. Sci.* **1999**, *420* (1), L122−L129.

(31) Riggs, W. M.; Parker, M. J. Surface analysis by X-ray photoelectron spectroscopy. In *Methods of Surface Analysis*; Czanderna, A. W., Ed.; Elsevier Publishing Company: Amsterdam, The Netherlands, 1975; pp 103−158.

(32) Schroeder, P. G.; France, C. B.; Parkinson, B. A.; Schlaf, R. J. *Appl. Phys.* **2002**, *91* (11), 9095−9107.

(33) Petrovykh, D. Y.; Kimura-Suda, H.; Tarlov, M. J.; Whitman, L. J. *Langmuir* **2004**, *20* (2), 429−440.

(34) Pope, M.; Swenberg, C. E. *Electronic Processes in Organic Crystals and Polymers*; Oxford University Press: Oxford, U.K., 1999.

(35) Schottky, W. *Naturwissenschaften* **1938**, *26*, 843.

(36) Mott, N. F. *Proc. Cambridge Philos. Soc.* **1938**, *34*, 568.